Interactive CardioVascular and Thoracic Surgery 27 (2018) 446–454
doi:10.1093/icvts/ivy044 Advance Access publication 22 March 2018

ORIGINAL ARTICLE

Cite this article as: Berdajs D, Mosbahi S, Eckstein FS, Charbonnier D, Ferrari E, von Segesser LK. Impact of the bicuspid aortic valve on aortic root haemodynamics: three-dimensional computed fluid dynamics simulation. Interact CardioVasc Thorac Surg 2018;27:446–54.

Impact of the bicuspid aortic valve on aortic root haemodynamics: three-dimensional computed fluid dynamics simulation†

Denis Berdajs[a,b,*], Selim Mosbahi[a], Friedrich S. Eckstein[b], Dominique Charbonnier[c], Enrico Ferrari[a] and Ludwig K. von Segesser[a]

[a] Department of Surgery and Anesthesiology, Cardiovascular Research, University Hospital Lausanne, Lausanne, Switzerland
[b] Department of Cardiac Surgery, University Hospital Basel, Basel, Switzerland
[c] CFS, Engineering Lausanne, Lausanne, Switzerland

* Corresponding author. Department of Cardiac Surgery, University Hospital Basel, Spitalstrasse 21, 4031 Basel, Switzerland. Tel: +41-61-2687180; fax: +41-61-2657324; e-mail: denis.berdajs@bluewin.ch (D. Berdajs).

Received 10 October 2017; received in revised form 2 December 2017; accepted 8 January 2018

Abstract

OBJECTIVES: The aim was to evaluate the impact of a bicuspid aortic valve (BAV) on local shear stress and on the pressure profile on the elements of the aortic root (AoR).

METHODS: The experiment setup included a BAV with aortic valve stenosis ($n = 5$ pigs, 67 ± 3.5 kg) and insufficiency ($n = 5$ pigs, 66.7 ± 4.4 kg). By implanting 6 high-fidelity microsonometric crystals in each AoR, we determined the 3-dimensional (3D) geometry of the AoR. Experimental and geometric data were used to create a 3D time- and pressure-dependent computed fluid dynamic model of the AoR with the BAV.

RESULTS: 3D AoR geometry was determined by AoR tilt (α) and rotation angle (β). Both values were maximal at the end of diastole: 24.41 ± 1.70° (α) and 20.90 ± 2.11° (β) for BAV with stenosis and 31.92 ± 11.51° (α) and 20.84 ± 9.80° (β) for BAV with insufficiency and minimal at peak ejection 23.42 ± 1.65° (α), 20.38 ± 1.61° (β) for stenosis and 26.62 ± 7.86° (α), 19.79 ± 8.45° (β) for insufficiency. In insufficiency, low shear stress of 0–0.08 Pa and moderate pressure (60–80 mmHg) were present. In BAV with stenosis, low shear stress of 0–0.5 Pa and moderate pressure (0–20 mmHg) were present at diastole; at peak ejection high shear stress >2 Pa and elevated pressure of >80 mmHg were present.

CONCLUSIONS: In a BAV with aortic valve stenosis, the haemodynamics are less favourable. The elevated pressure with elevated shear stress may over the long term promote degenerative processes in the leaflets and consequently valve function failure.

Keywords: Aortic valve stenosis • Aortic valve insufficiency • Aortic root • Computed fluid dynamic simulation

INTRODUCTION

The bicuspid aortic valve (BAV), which represents the most common congenital heart defect, has been associated with aortic wall dilatation, aneurysm formation and dissection [1–3]. Even in a normally functioning BAV, aortic wall disease most frequently targets the ascending aorta [4, 5]. The exact mechanism behind the disruption of aortic wall integrity is the subject of ongoing discussion. The haemodynamic hypothesis puts forth the idea that altered aortic valve anatomy is a key factor in pathological flow characteristics and thus is a cause of aortic wall disease [6–8]. However, complex flow conditions per se were not only associated with the BAV but were also considered to be the source of the pathological processes occurring at the ascending aorta in a tricuspid aortic valve [6]. There is growing evidence that the BAV influences flow conditions in the ascending aorta [9–11], which results in pathological shear stress and wall pressure profiles. The shear stress and pressure alterations form normal patterns that may be considered as important trigger factors for a degenerative process in the aortic wall.

Despite investigations on the impact of the BAV on flow conditions in the aorta using sophisticated and technically demanding approaches [10, 11], the effects of the pattern of local haemodynamic conditions on aortic root (AoR) elements with BAV have only been evaluated in a few reports [10, 12]. The mechanism of the relatively early degeneration of the BAV compared to that of the tricuspid aortic valve has not been investigated in all its facets. The link between AoR 3-dimensional (3D) deformation and haemodynamic performance has been described previously. A novel numerical approach defining the AoR as a 3D geometrical shape was introduced [13]. A similar analysis was applied in a recent report aimed at defining the spatial

†Presented at the 31st Annual Meeting of the European Association for Cardio-Thoracic Surgery, Vienna, Austria, 7–11 October 2017.

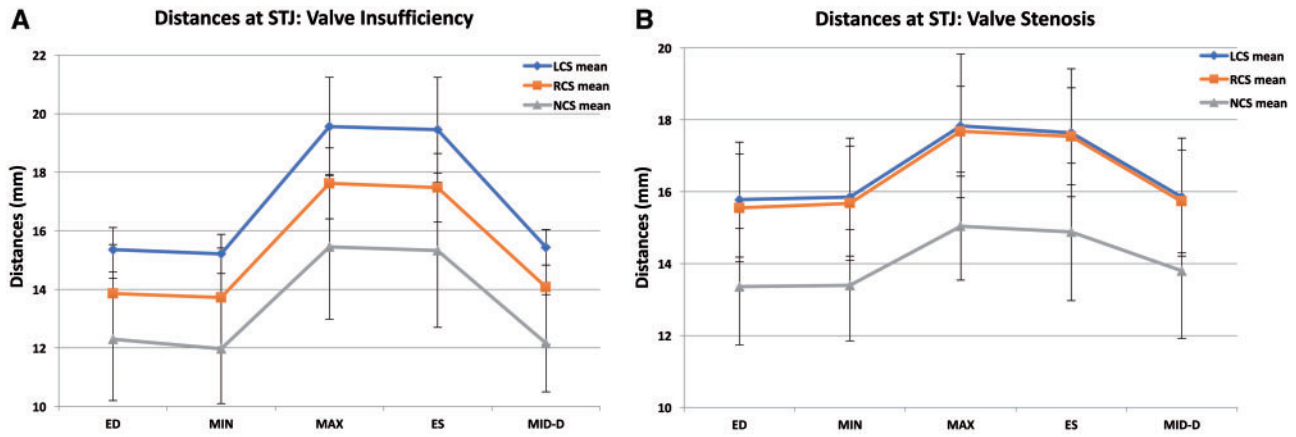

Figure 1: Distances between the 3 commissures in the bicuspid aortic valve with valve insufficiency (**A**) and in the bicuspid aortic valve with valve stenosis (**B**). In both morphological modalities, the distances measured at the LCS and RCS are similar and larger than those measured at the NCS ($P > 0.05$). ED: end diastole; ES: end of systole; LCS: left coronary sinus; Max: maximal/peak ejection; Mid-D: mid-term of diastole at mitral valve opening; Min: end of the isovolaemic contraction; NCS: non-coronary sinus; RCS: right coronary sinus; STJ: sinotubular junction.

deformation of the AoR with BAV. Our computed fluid dynamics (CFD) simulation, based on experimental and geometric data, provided time- and pressure-dependent local shear stress and pressure profiles of the BAV with valve stenosis and insufficiency.

MATERIALS AND METHODS

Animal protocol

The research protocol was approved by the local committee on animal care of the Office Vétérinaire Cantonal, Lausanne Switzerland. The mean body weight of the animals was as follows: BAV with aortic valve stenosis, 67 ± 3.5 kg ($n = 5$ domestic pigs) and BAV with aortic valve insufficiency, 66.7 ± 4.4 kg ($n = 5$ domestic pigs). The methods, including a description of the 3D geometry of the AoR, and the CFD simulation, were described previously [13]. Briefly, monitoring was performed using a jugular venous catheter for central venous pressure, invasive arterial pressure at the femoral artery and 5-lead echocardiography [13]. Cardiopulmonary bypass was established by a 26-Fr venous cannula (SmartCannula®, Lausanne, Switzerland) in the right atrium and a 2-Fr cannula (Eopa® cannula, Medtronic Inc., Minneapolis, MN, USA) at the aortic arch. Full systemic heparinization (activated clotting time >480 s) was used throughout the procedure. After the ascending aorta was cross-clamped, the aorta was opened superior to the sinotubular junction (STJ). Subsequently, the tricuspid aortic valve was transformed into a BAV Type I. A BAV was created by suturing the conjoined coaptation between the left and right coronary leaflets. Stenosis of the valve was created in 5 consecutive animals by partial suture of the coaptation between the left and non-coronary leaflet coaptation, as well with partial suture of the coaptation between the right and non-coronary leaflet coaptation. Insufficiency was obtained in 5 animals by removing the lunula of the non-coronary leaflets.

In each AoR, high-resolution ultrasonic crystals (2 mm, 200 Hz, Sonometrics Corporation, London, ON, Canada) were implanted at 3 commissures and at their projection at the level of the AoR base. Pressure at the ascending aorta and left ventricle was obtained by high-fidelity catheter-tipped pressure transducers (Millar Instruments, Houston, TX, USA) [13, 14]. After the animals were weaned from the cardiopulmonary bypass and haemodynamic stability was established, 10 registrations of 10 min each were done. At the end of the experiment, the heart was explanted, and an autopsy was performed to confirm the correct position of all 6 crystals [13, 14].

3-dimensional geometry during the cardiac cycle

Cardiac cycle-related 3D AoR geometric deformation was assessed at the following times: (i) the beginning of isovolaemic contraction, (ii) aortic valve opening, (iii) peak ejection, (iv) end of systole, when the aortic valve closes and at (v) the end of isovolaemic relaxation at the lowest pressure value in the left ventricle when the mitral valve opens [15].

The 3D AoR geometry is defined as an oblique triangular prism [12, 16]. The upper triangle corresponds to the level of the STJ; the 3 points of the triangle [intervalvular triangle (IVT)] are at the anterior, right and left commissures. The inferior triangle is at the level of the AoR base, and the edge points correspond to the vertical projections of the 3 commissures to the base of individual IVT [13, 14, 16].

Data acquisition and definition of 3-dimensional deformation

Measured distances between the crystals and left ventricular and ascending aorta pressures were synchronized using Digital Sonomicrometer System software (Sonometrics Corporation). Time and pressure-related 3D deformation of the AoR was defined through post-measurement data processing (CardioSoft program, Sonometrics Corporation). The following distances were measured: (i) intercommissural distances, (ii) the distance between crystals at the base of the AoR, (iii) the vertical distances corresponding to the height of each IVT and (iv) the diagonal distances corresponding to the diagonal deformation of each sinus. The radius at the STJ and the AoR base was calculated according to Euclidian space rules [13, 14, 17].

Definition of aortic root tilt and torsion angle

The AoR tilt angle (α) was defined as the angle between the STJ and the AoR base. Defining the origin (0, 0, 0) of the *x*-*y*-*z* 3D

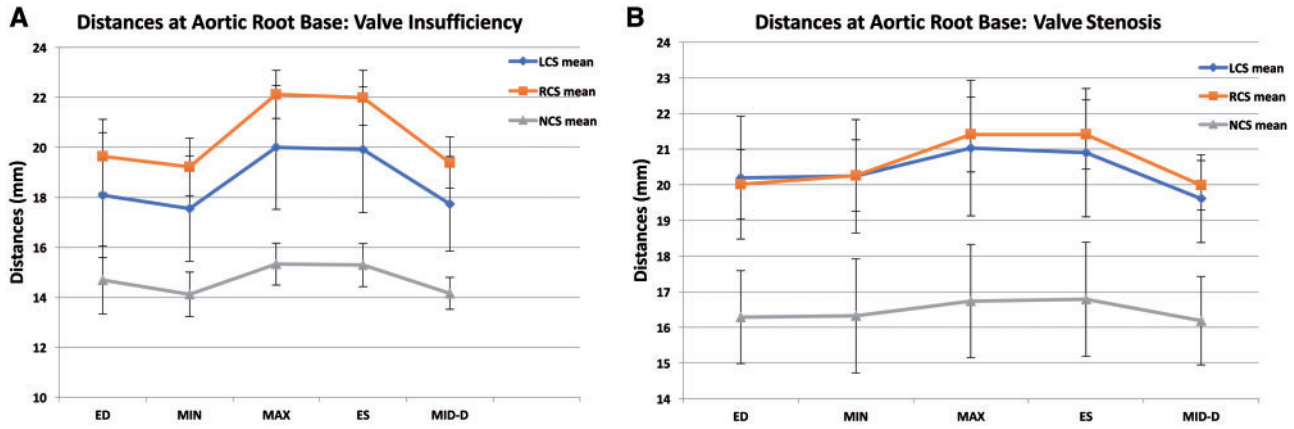

Figure 2: Distance between the intervalvular triangle base in bicuspid aortic valve with valve insufficiency (**A**) and in bicuspid aortic valve with valve stenosis (**B**). In both morphological modalities, the distances at the LCS and RCS are similar and larger than those measured at the NCS ($P > 0.05$). ED: end diastole; ES: end of systole; LCS: left coronary sinus; Max: maximal/peak ejection; Mid-D: mid-term of diastole at mitral valve opening; Min: end of the isovolaemic contraction; NCS: non-coronary sinus; RCS: right coronary sinus.

coordinate system in the middle of the non-coronary sinus (NCS), the tilt angle corresponds to the angle between the STJ plane and the *z*-*y* plane [17, 18]. The rotation angle (β) was defined as rotation around the *z*-axis of the AoR base and the STJ plane [13, 14].

Statistical analysis of measured data

Data are presented as mean and standard deviation. Statistical analysis was done with SciPy 0.18.0 (Python Software Foundation scientific library, Beaverton, OR, USA). Changes in measured parameters during the cardiac cycle were tested for significance using 2-sample (unpaired) *t*-tests. The mean values of the intercommissural and basal distances were compared, with a *P*-value <0.05 rejecting the null hypothesis.

Computed fluid dynamic modelling of the aortic root

A CFD model of BAV with stenosis and insufficiency was established to evaluate local pressure and shear stress profiles. The corresponding geometry of each BAV AoR modality was designed based on experimental data. The dimensions of the AoR prism (as defined per the sonomicrometric crystals) were used to build 8 geometric models in accordance with the cardiac cycle and time-set values. A discretized set of 100 geometrical models was interpolated and generated in order to reproduce the geometric deformation of the AoR and the movement of the 3 leaflets during the complete cardiac cycle as mentioned previously [13, 14]. The ANSYS ICE MCFD (ANSYS Inc., Canonsburg, PA, USA) preprocessor tool was used to generate the multiblock structured grids needed by the Navier–Stokes Multi Block flow solver. An O-grid topology (which aligns the hexahedral cells of the structured grid with the walls of the geometric model) was used to refine the mesh close to the walls in order to correctly capture the laminar boundary layer in these regions [13, 14]. The grid for the AoR comprises 308 structured blocks for around 1.8 million cells. Blood was modelled as a Newtonian fluid with a viscosity of 4×10^{-3} Pa and a density of 1060 kg/m^3. On the AoR wall, and on 3 leaflets, no-slip boundary conditions were imposed. A pulsatile velocity flow profile, pressure at the left ventricle and ascending aorta pressure were applied according to measured values from the experimental scenario. The Navier–Stokes Multi Block solver uses a cell-centred finite volume method to solve the compressible Navier–Stokes equations [13, 14]. Spatial discretization was ensured by a 4th-order central scheme, and time discretization was resolved by an implicit scheme [13–15, 19].

RESULTS

BAV with valve stenosis and valve insufficiency was created successfully in all animals. After the animal was weaned from cardiopulmonary bypass and stable haemodynamic conditions were achieved, recordings were performed 10 times over a period of 10 min. Ten consecutive cardiac cycles were chosen for analysis.

In aortic valve stenosis, the invasively measured steady-state pressure values were as follows: mean systolic pressure 87.61 ± 6.61 mmHg, mean diastolic pressure 71.33 ± 8.13 mmHg. For valve insufficiency, the mean systolic pressure was 79.66 ± 7.97 mmHg and the mean diastolic pressure was 38.33 ± 10.47 mmHg. In BAV with insufficiency, the mean transvalvular gradient at ejection was 21.19 ± 8.55 mmHg and at diastole, it was 18.69 ± 4.57 mmHg whereas in stenosis, at ejection it was 49.24 ± 3.55 mmHg and at diastole it was 39.04 ± 4.24 mmHg.

3-Dimensional geometry of the aortic root during a cardiac cycle

The expansion of the left coronary sinus (LCS), the right coronary sinus (RCS) and the NCS in BAV with stenosis and insufficiency showed the following patterns: The intercommissural distances of the LCS and RCS in BAV with insufficiency were as follows: maximal distance at peak ejection, 19.56 ± 1.68 for LCS, 17.62 ± 1.21 for RCS and 15.45 ± 2.47 for NCS ($P < 0.05$) minimal distance at the end of isovolaemic relaxation, 15.43 ± 0.60 for LCS, 14.08 ± 1.96 for RCS and 12.16 ± 1.66 for NCS ($P < 0.05$) (Fig. 1). A similar pattern of intercommissural distances was noted in BAV with stenosis (Fig. 1). The maximal distance at peak ejection was 17.83 ± 2.00 for LCS, 17.68 ± 1.25 for RCS and 15.04 ± 3.00 for NCS ($P < 0.05$); the minimal distance at the end of isovolaemic

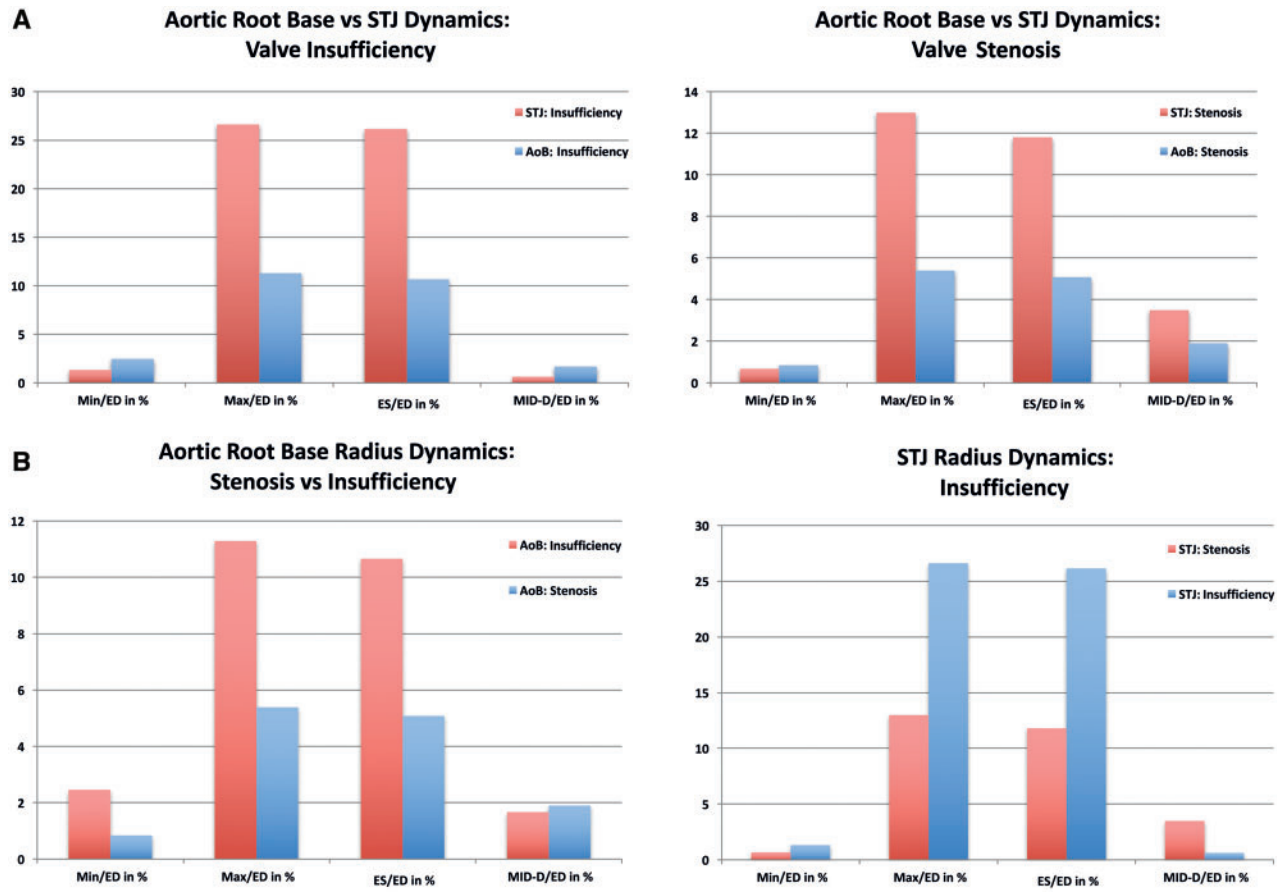

Figure 3: Radius changes at aortic root base and sinotubular junction in bicuspid aortic valve with valve insufficiency and in stenosis (**A**). Relative changes in both aortic root modalities at the AoR base and STJ (**B**). AoR: aortic root; ED: end diastole; ES: end of systole; Max: maximal/peak ejection; Mid-D: mid-term of diastole at mitral valve opening; Min: end of the isovolaemic contraction; STJ: sinotubular junction.

relaxation was 15.85 ± 1.64 for LCS, 15.73 ± 1.43 for RCS and 13.80 ± 2.88 for NCS ($P < 0.05$) (Fig. 1).

A similar pattern was observed at the base of the AoR. In BAV with insufficiency, the maximal distances occurred at peak ejection: 20.00 ± 2.48 mm for LCS, 22.12 ± 0.96 mm for RCS and 15.33 ± 0.84 for NCS ($P < 0.05$); the smallest distances occurred at the end of isovolaemic relaxation: 17.74 ± 1.89 mm for LCS, 19.39 ± 1.03 mm for RCS and 14.16 ± 0.64 mm for NCS ($P < 0.05$). In BAV with stenosis, expansion of the LCS and RCS base was identical and larger than expansion of the NCS base. Maximal expansion occurred at peak ejection: 17.64 ± 1.78 mm for LCS, 17.54 ± 1.35 mm for RCS and 14.88 ± 2.91 mm for NCS ($P < 0.05$) (Fig. 2).

In BAV with insufficiency, the relative radius deformation at the STJ was larger, as at the AoR base. Compared to the baseline value at the end of diastole, the largest expansion was noted at peak ejection: 26.62 ± 4.37% for the STJ and 11.29 ±4.46% for the AoR base. The smallest expansion occurred at the end of the isovolaemic contraction: 0.62 ± 2.84% for the STJ and 1.67 ± 0.3% for the AoR base (Fig. 3). In BAV with stenosis, the deformation of the radius at the STJ was larger than at the AoR base. The largest expansion was at the peak ejection: 12.99 ± 4.01% for the STJ and 5.39 ± 0.33% for the AoR base and smallest at end of the isovolaemic contraction: 0.84 ± 1.40% for the STJ and 0.67 ± 1.40% for the AoR base (Fig. 3).

The AoR tilt angle (α) is defined as the angle between the STJ and AoR base plane, whereas the rotation (β) angle is a horizontal displacement of the STJ over the AoR base. In BAV with insufficiency, the tilt angle (α) reached its maximal value at the end of the isovolaemic contraction, 31.90 ± 1.15° and its minimal value at peak ejection at 26.98 ± 0.78°. At closure of the aortic valve, it was 26.98 ± 0.82°. From here on it increased; at closure of the mitral valve, it was 31.2 ± 1.07°. In BAV with stenosis, a similar pattern in tilt angle dynamics was observed, with a maximal value at the end of an isovolaemic contraction of 24.41 ± 1.72°, minimal values at a peak ejection of 23.4 ± 1.65° and at an aortic valve closure of 23.5 ± 1.64°. From here on, the tilt angle increased again up to the value measured at the end of the diastole, 24.26 ± 1.7° (Fig. 4).

The AoR rotation angle (β) pattern was as follows: In BAV with insufficiency, it reached its maximal value at the end of the isovolaemic contraction, 21.47 ± 0.90°, and its minimal value at peak ejection, 19.79 ± 0.85°. From here on, the angle increased, and, at closure of the mitral valve, it was 20.84 ± 0.98°. In BAV with stenosis, the rotation angle was as follows: maximal value at the end of isovolaemic contraction, 21.10 ± 1.72°, and minimal at peak ejection, 20.38 ± 1.61° and aortic valve closure, 19.92 ± 0.84°. From here on, the rotation angle increased up to the value measured at the end of diastole, 20.9 ± 1.73° (Fig. 4).

Computational fluid dynamics simulation of the bicuspid aortic root

Shear stress profile. In BAV with insufficiency, AoR components such as the IVT, 3 commissures, the lunula, the valve hinge region

EXPERIMENTAL

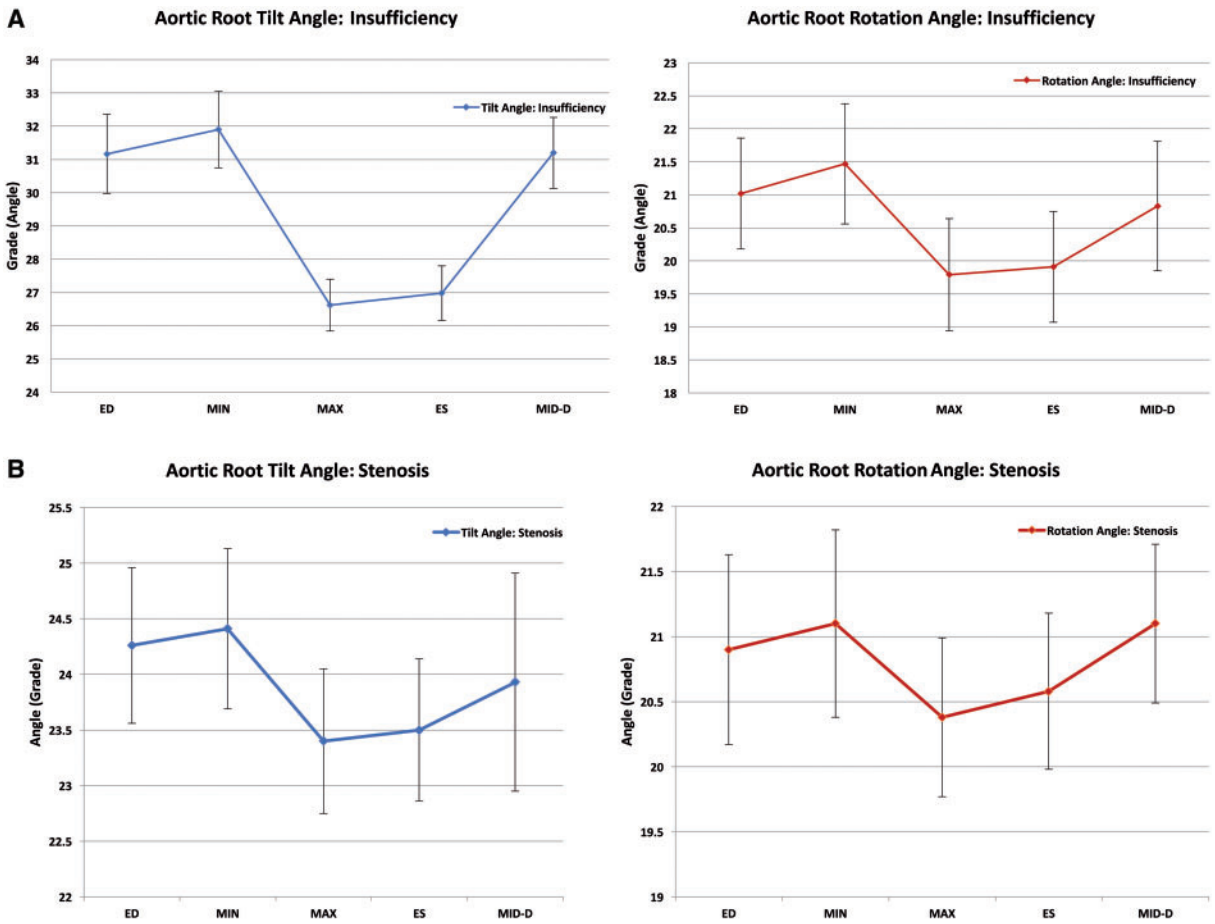

Figure 4: Tilt and rotation angle in insufficiency (**A**) and in stenosis (**B**). ED: end diastole; ES: end of systole; Max: maximal/peak ejection; Mid-D: mid-term of diastole at mitral valve opening; Min: end of the isovolaemic contraction.

and the body of the leaflets were exposed to low shear stress ranging between 0 and 0.5 Pa. At peak ejection, the lunula, the 3 commissures and the superior part of the IVTs were in a moderate shear stress of 0.5–1.4 Pa. At the end of systole, the middle region of the leaflets was exposed to a moderate to high shear stress of 0.5–1.8 Pa. In BAV with stenosis, the following shear stress pattern was observed: At the end of diastole and at the end of the isovolaemic contraction, the IVT, the valve hinge region and the body of the leaflets were exposed to a low shear stress of 0–0.5 Pa. The lunula at the 3 commissures was exposed to high shear stress >2 Pa. At peak ejection the lunula, the 3 commissures, the superior one-third of the leaflets and the superior part of IVT were exposed to high shear stress >2 Pa. At fusion of the 2 leaflets, more than half of the leaflet surface was in high shear stress >2 Pa. At valve closure, AoR components were in a low shear stress range of 0–0.5 Pa with the exception of the lunula (Fig. 5, Video 1).

Pressure profile. The pressure profile on the surface of the AoR components was as follows: In BAV with insufficiency, at the end of diastole and at the end of isovolaemic contraction, the pressure was in a moderate range of 50–70 mmHg. At peak ejection, the lunula was exposed to a moderately high pressure of 70–80 mmHg, whereas the rest of the AoR was in a moderate pressure range of 50–70 mmHg. From the end of systole to the end of diastole, a moderate pressure profile of 50–70 mmHg was found again.

In BAV with stenosis, at the end of diastole and isovolaemic contraction, AoR components were exposed to a low pressure of 0–30 mmHg. At peak ejection, the 3 commissures, the 3 IVTs, the valve bodies and the nadir were exposed to a moderate pressure of 50–70 mmHg. Nadirs were exposed to a low pressure load of 0–30 mmHg. From closure of the aortic valve, the lunula, the 3 commissures, the 3 IVTs, the valve bodies and the nadirs were exposed to low pressure (Fig. 6, Video 2).

DISCUSSION

This experimental study provided numerical 3D real-time and pressure-dependent shear stress and pressure profile analysis of the AoR with BAV in aortic valve stenosis and insufficiency. Elevated shear stress and pressure at the surface of the leaflets was registered during the whole period of ejection in BAV with valve stenosis. This occurs at valve coaptation, at the 3 commissures and at the superior one-third of the valve body. In addition to the mentioned regions, a large area is exposed to elevated shear stress at the fusion of conjoined leaflets, where the effective valve stenosis was created. Importantly, there is rapid pressure and shear stress augmentation at the mentioned regions at the transition from the end of isovolaemic contraction to the effective ejection phase. This process occurs with a factor >2 for shear stress and a

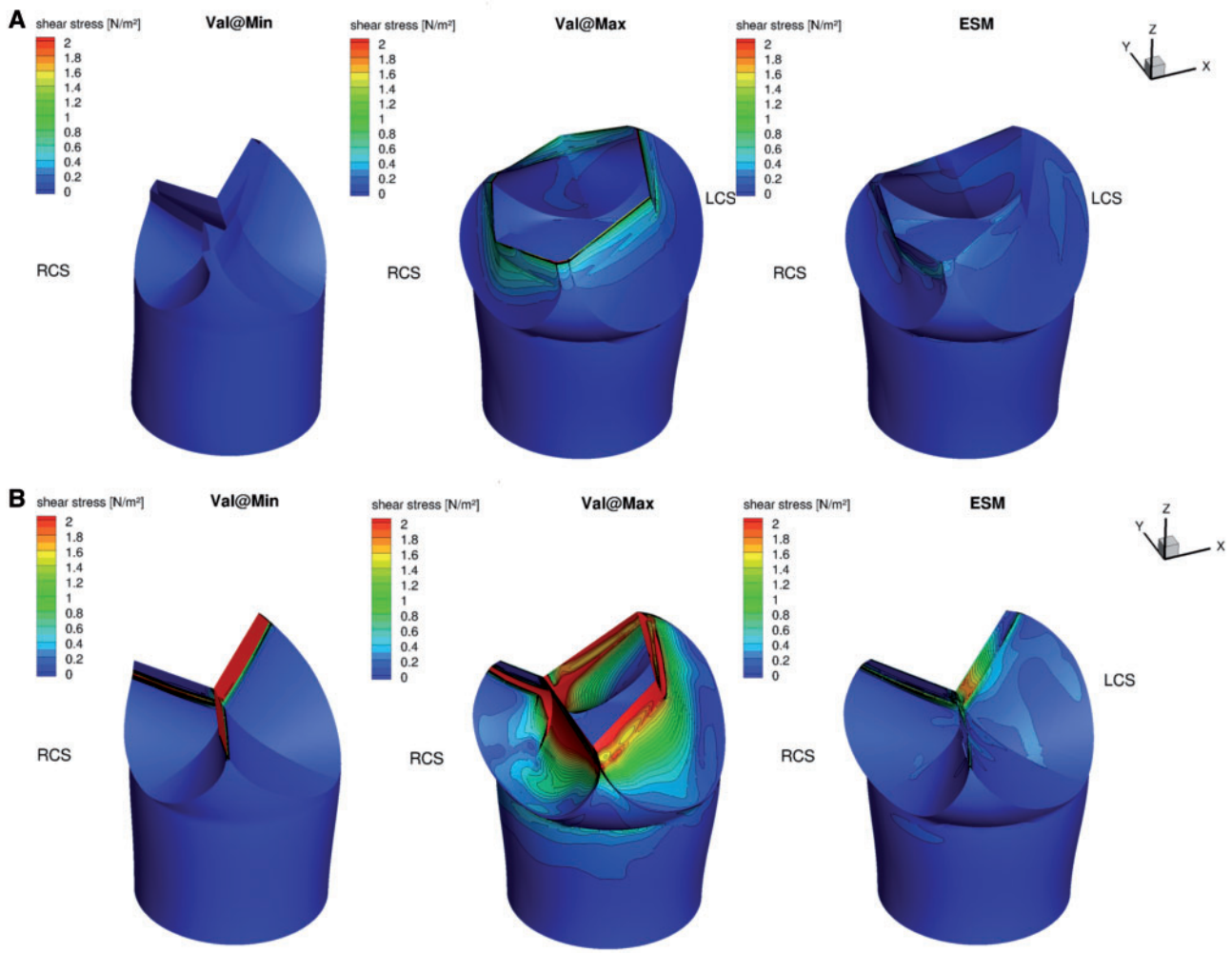

Figure 5: Shear stress profile in insufficiency (**A**) and stenosis (**B**). LCS: left coronary sinus; Max: maximal/peak ejection; Min: end of the isovolaemic contraction; RCS: right coronary sinus.

factor of 2–30 for the pressure profile. Note that from the period of aortic valve closure to the ejection, the elements of the AoR are exposed to low shear stress and pressure. Findings in valve insufficiency were less spectacular. Pressure and shear stress oscillation from diastole to systole were practically not registered. In BAV with insufficiency, the AoR components were exposed to elevated pressure during the whole cardiac cycle. This may not be surprising, because aortic valve closure does not occur, and the elevated pressure is de facto a consequence of the equilibration of the hydraulic pressure between the ascending aorta and the left ventricle. The shear stress for BAV with insufficiency was in a low range.

AoR has a complex 3D morphology, and the spatial relation of its elements and their natural shape alterations results finally in an asymmetric geometric pattern. When one is studying the complex 3D relations, it may be self-explanatory that each individual element is an essential contributor in its normal function. In fact, AoR 3D dynamics comprise a sequence of well-defined and precise interactions of the AoR components during the cardiac cycle. The geometric 3D deformation of the AoR may be defined by 2 global parameters, the tilt and rotation angles. This numerical approach, which was defined previously [13], was also used in a recent analysis as a bench model to evaluate the impact of the BAV on haemodynamic conditions in an individual AoR. When comparing our CFD simulation, which is based on 4-dimensional (4D) time, pressure-related geometry and invasive pressure and flow measurements, we emphasize that our approach reflects the real local shear stress and pressure conditions as accurately as possible. In contrast, in the recent literature, the finite simulation of the elements of the BAV [10–12] and their effects on flow and shear stress are mostly supported by non-invasive diagnostic tools (such as 4D magnetic resonance imaging) that, in fact, do not reflect real-time flow and pressure-dependent 4D AoR deformation. The simulations are in some instances based on mathematical calculations and approximations of the local haemodynamic conditions [10, 12, 13].

Analogous to the native geometry in BAV with insufficiency or stenosis, 3D deformation of the AoR changes from a tilted cone at diastole to almost a straight cylinder-like geometry at ejection [13]. This almost cylinder-like form brings the left ventricular outflow tract, the AoR and the ascending aorta into almost straight alignment. This process occurs with the one goal of minimizing resistance on AoR components during the short phase of large-volume blood flow. Based on the analysis of the geometry of the BAV, it seems that the morphology of the aortic valve per se does not influence in a global manner the 3D geometry of the AoR that is similar to the deformation in native AoR [13]. Consequently, one would conclude that the haemodynamic profile of shear stress and pressure in BAV with stenosis or insufficiency would not alter

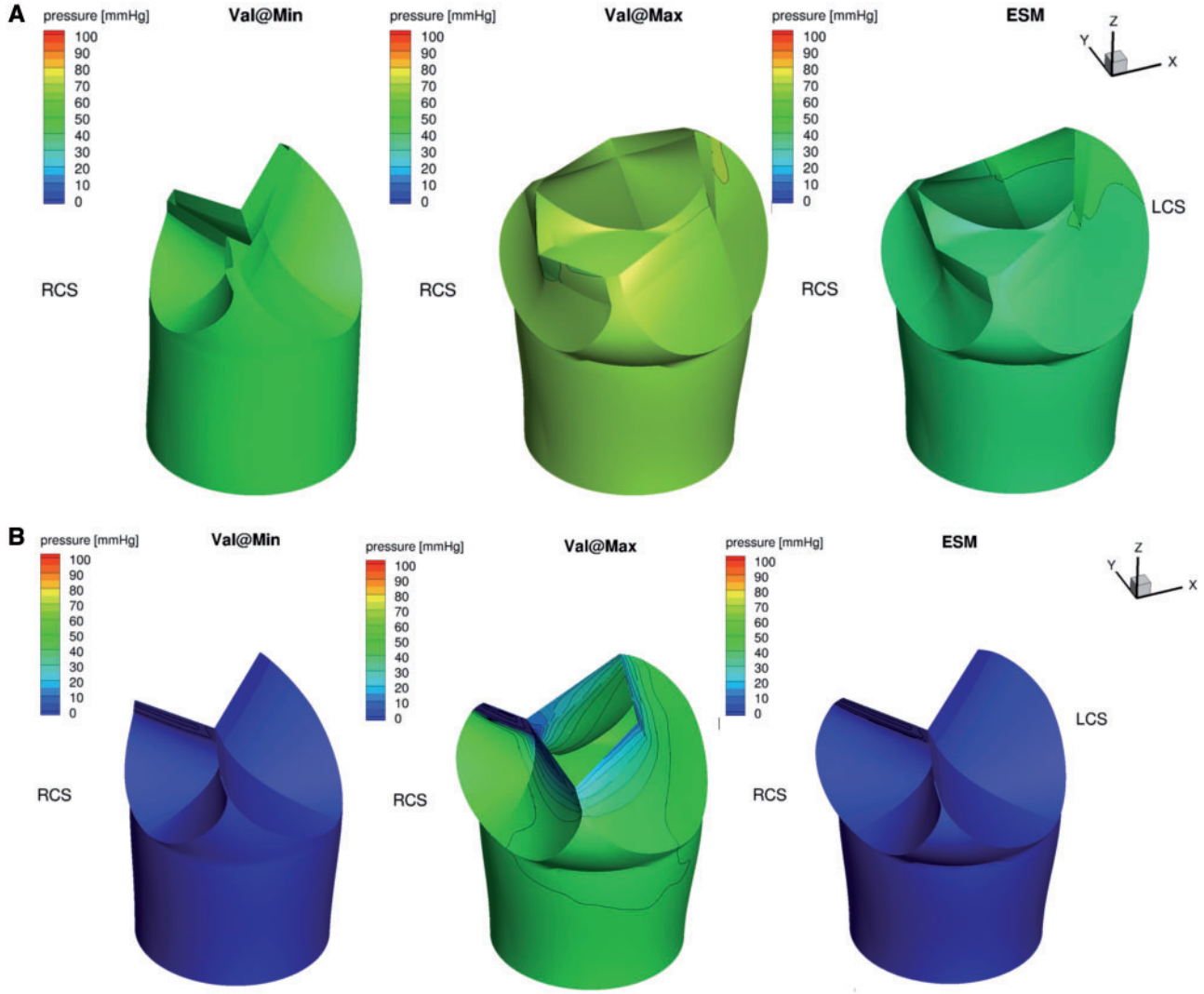

Figure 6: Local pressure in bicuspid aortic valve with valve insufficiency (**A**) and stenosis (**B**). LCS: left coronary sinus; Max: maximal/peak ejection; Min: end of the isovolaemic contraction; RCS: right coronary sinus.

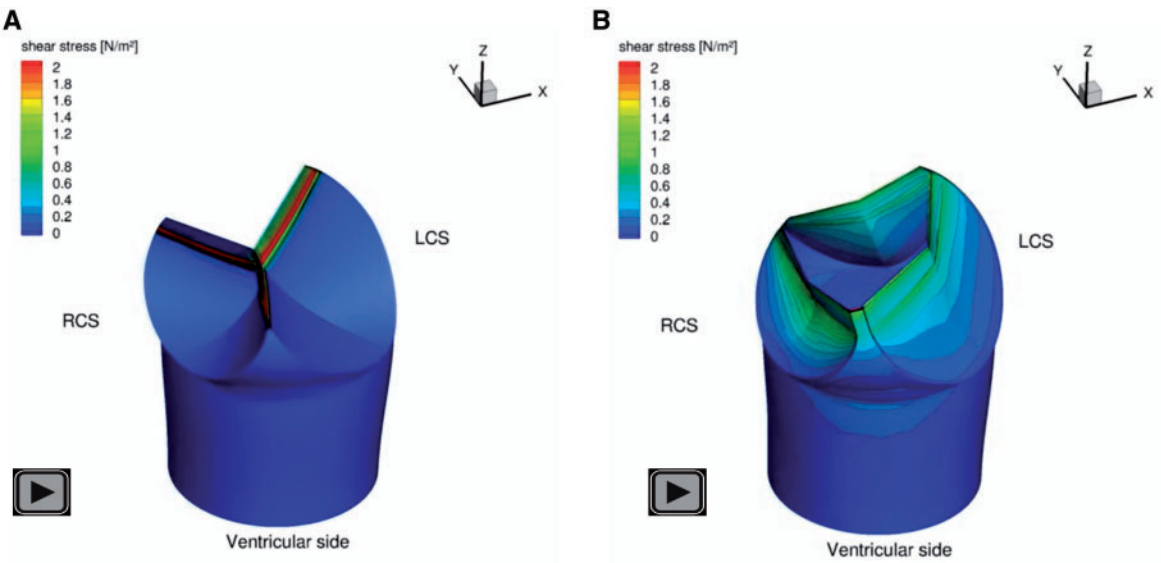

Video 1: Shear stress profile in bicuspid aortic valve with stenosis (**A**) and insufficiency (**B**).

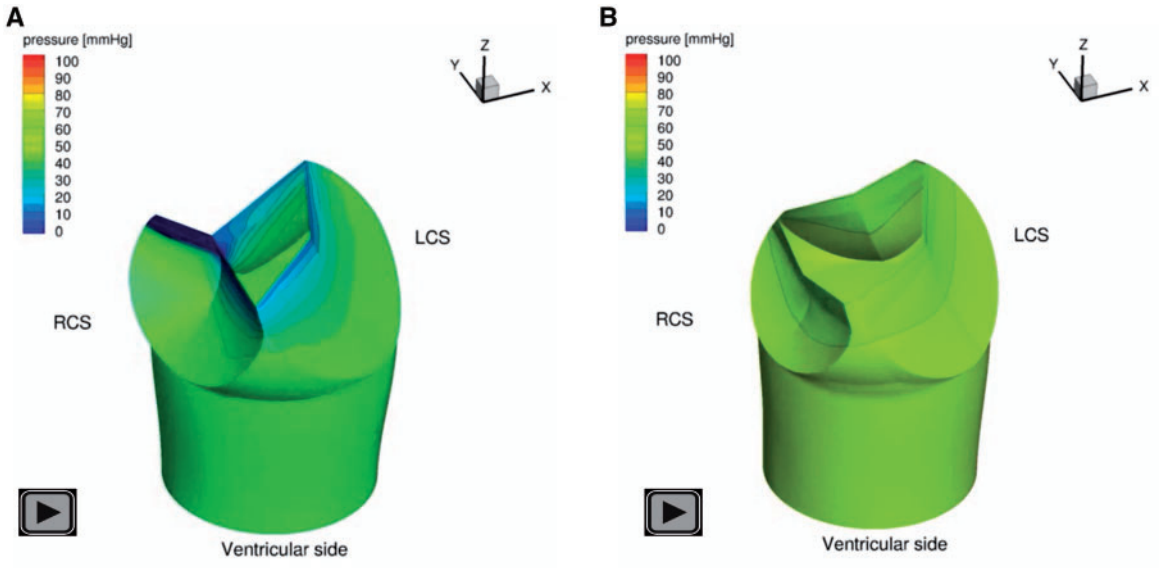

Video 2: Pressure profile in bicuspid aortic valve with stenosis (**A**) and insufficiency (**B**).

tremendously from that in the native AoR [13]. This conclusion is, however, only partly true: In BAV with insufficiency, the pressure and shear stress remain in low ranges during the entire cardiac cycle and, as such, most closely approach the haemodynamics of the native artic root. This situation does not prevail in valve stenosis, where the pressure and the shear stress demonstrate prompt augmentation at the ejection phase. Because the elevated shear stress and pressure augmentation on the surface of the vascular wall are considered as strong predictive factors for vessel wall degeneration and development of sclerosis, one may suppose that the BAV with stenosis would undergo a degenerative process. Consequently, the sclerotic process that occurs at the region of leaflet fusion and the commissures would lead to the deterioration of valve mobility [20, 21] and the grade of stenosis.

Clearly, our results were obtained from an experimental trial with its associated limitations, which include the acute and open chest nature of the experiments, the relative myocardial ischaemia and the invasive nature of the experiments. One should consider that the accuracy of the experimental results differs from that obtained from natural congenital BAV stenosis, the insufficiency of its morphology and the duration, which actually is a long-lasting condition. We recognize that valve disease created in an experimental setting does not correspond in all details to the actual congenital condition. Therefore, we believe that long-term animal experiments would shed light on the details of the pathological aspects of congenital BAV.

However, we emphasize that, using a method that was described and validated previously, the results of these experiments established a link between BAV disease and local haemodynamic conditions. We strongly believe that our results provide insight into the haemodynamic impact of the BAV, both locally and also in a global time-dependent manner. As such, based on recent analyses, one may consider a BAV aortic valve with a stenotic component as a precursor of valve degeneration that, at some point, is an indication for elective valve intervention. Further, the data presented may be considered when designing a reconstructive procedure for BAV such as in reimplantation and leaflet reconstruction. Namely, any post-procedural residual stenosis may result in pathological local haemodynamic conditions that would lead to failure of the neo leaflets. However, this hypothesis needs further experimental and clinical evaluation.

Conflict of interest: none declared.

REFERENCES

[1] Bonow RO. Bicuspid aortic valves and dilated aortas: a critical review of the ACC/AHA practice guidelines recommendations. Am J Cardiol 2008; 102:111–4.
[2] Michelena HI, Khanna AD, Mahoney D, Margaryan E, Topilsky Y, Suri RM *et al*. Incidence of aortic complications in patients with bicuspid aortic valves. JAMA 2011;306:1104–12.
[3] Hahn RT, Roman MJ, Mogtader AH, Devereux RB. Association of aortic dilation with regurgitant, stenotic and functionally normal bicuspid aortic valves. J Am Coll Cardiol 1992;19:283–8.
[4] Keane MG, Wiegers SE, Plappert T, Pochettino A, Bavaria JE, Sutton MG. Bicuspid aortic valves are associated with aortic dilatation out of proportion to coexistent valvular lesions. Circulation 2000;102:III35–9.
[5] den Reijer PM, Sallee D, van der Velden P, Zaaijer ER, Parks WJ, Ramamurthy S *et al*. Hemodynamic predictors of aortic dilatation in bicuspid aortic valve by velocity-encoded cardiovascular magnetic resonance. J Cardiovasc Magn Reson 2010;12:4.
[6] Poullis MP, Warwick R, Oo A, Poole RJ. Ascending aortic curvature as an independent risk factor for type dissection, and ascending aortic aneurysm formation: a mathematical model. Eur J Cardiothorac Surg 2008; 33:995–1001.
[7] Beller CJ, Labrosse MR, Thubrikar MJ, Robicsek F. Finite element modeling of the thoracic aorta: including aortic root motion to evaluate the risk of aortic dissection. J Med Eng Technol 2008;32:167–70.
[8] Robicsek F, Mano J. Hemodynamic considerations regarding the mechanism and prevention of aortic dissection. Ann Thorac Surg 1994;58: 1247–53.
[9] Bauer M, Siniawski H, Pasic M, Schaumann B, Hetzer R. Different hemodynamic stress of the ascending aorta wall in patients with bicuspid and tricuspid aortic valve. J Cardiac Surgery 2006;21:218–20.
[10] Barker AJ, Markl M, Bürk J, Lorenz R, Bock J, Bauer S *et al*. Bicuspid aortic valve is associated with altered wall shear stress in the ascending aorta. Circ Cardiovasc Imaging 2012;5:457–66.
[11] Schnell S, Smith DA, Barker AJ, Entezari P, Honarmand AR, Carr ML *et al*. Altered aortic shape in bicuspid aortic valve relatives influences blood flow patterns. Eur Heart J Cardiovasc Imaging 2016;17:1239–47.

[12] Cao K, Sucosky P. Effect of bicuspid aortic valve cusp fusion on aorta wall shear stress: preliminary computational assessment and implication for aortic dilation. World J Cardiovasc Dis 2015;05:129–40.
[13] Berdajs D, Mosbahi S, Forro Z, Ferrari E, Charboniere D, von Segesser LK. Numerical analysis of the 3-dimensional aortic root morphology during the cardiac cycle. Eur J Cardiothorac Surg 2016;49:1213–2121.
[14] Berdajs D, Mosbahi S, Forro Z, Burki M, von Segesser LK. Aortic root haemodynamics following David procedure: numerical analysis of 3-dimensional haemodynamics. Eur J Cardiothorac Surg 2016;49:1588–98.
[15] Vos JB, Leyland P, van Kemenade V, Gacherieu C, Duquesne N, Lötstedt P. NSMB Handbook 6.07. 2014, 601–97.
[16] Berdajs D, Patonay L, Turina M. Clinical anatomy of the aortic root. Cardiovasc Surg 2002;10:320–7.
[17] Dörrie H. 100 Great Problems of Elementary Mathematics. Dover, 1965.
[18] Weisstein EW. "Conical Frustum." From *MathWorld*–A Wolfram Web Resource.
[19] Vos J, Rizzi A, Corjon A, Chaput E, Soinne E. Recent advances in aerodynamics inside the NSMB (Navier-Stokes Multi-Block) consortium. AIAA Paper 1998;802:1998–9.
[20] Traub O, Berk BC. Laminar shear stress: mechanisms by which endothelial cells transduce an atheroprotective force. Arterioscler Thromb Vasc Biol 1998;18:677–85.
[21] Chatzizisis YS, Coskun AU, Jonas M, Edelman ER, Stone PH, Feldman CL. Risk stratification of individual coronary lesions using local endothelial shear stress: a new paradigm for managing coronary artery disease. Curr Opin Cardiol 2007;22:552–64.